Bulletin of the Seismological Society of America, Vol. 99, No. 5, pp. 2721–2735, October 2009, doi: 10.1785/0120080268

A Case Study of Two M ~5 Mainshocks in Anza, California: Is the Footprint of an Aftershock Sequence Larger Than We Think?

by Karen R. Felzer and Debi Kilb

Abstract It has been traditionally held that aftershocks occur within one to two fault lengths of the mainshock. Here we demonstrate that this perception has been shaped by the sensitivity of seismic networks. The 31 October 2001 M_w 5.0 and 12 June 2005 M_w 5.2 Anza mainshocks in southern California occurred in the middle of the densely instrumented ANZA seismic network and thus were unusually well recorded. For the June 2005 event, aftershocks as small as M 0.0 could be observed stretching for at least 50 km along the San Jacinto fault even though the mainshock fault was only ~4.5 km long. It was hypothesized that an observed aseismic slipping patch produced a spatially extended aftershock-triggering source, presumably slowing the decay of aftershock density with distance and leading to a broader aftershock zone. We find, however, the decay of aftershock density with distance for both Anza sequences to be similar to that observed elsewhere in California. This indicates there is no need for an additional triggering mechanism and suggests that given widespread dense instrumentation, aftershock sequences would routinely have footprints much larger than currently expected. Despite the large 2005 aftershock zone, we find that the probability that the 2005 Anza mainshock triggered the M 4.9 Yucaipa mainshock, which occurred 4.2 days later and 72 km away, to be only 14% ± 1%. This probability is a strong function of the time delay; had the earthquakes been separated by only an hour, the probability of triggering would have been 89%.

Online Material: Movies exploring the spatial extent of aftershocks from the 2001 and 2005 Anza sequences.

Introduction

The relationship between a mainshock and its aftershocks has been a topic of study for decades (Omori, 1894; Benioff, 1951; Utsu, 1961; Scholz, 1968; Nur and Booker, 1972; Das and Scholz, 1981; Dieterich, 1994; Toda *et al.*, 1998; Kilb *et al.*, 2000; Parsons, 2005; Helmstetter and Shaw, 2006; Hill, 2008), yet many basic questions about the physics of aftershock triggering remain unresolved (Gomberg, 2001). For example, we do not know the underlying physics of how one earthquake triggers another, nor is there consensus on the distance extent between a typical aftershock and the triggering mainshock. Until the early 1990s it was commonly believed that all triggered earthquakes occurred within a zone of one to two mainshock fault lengths from the mainshock hypocenter (Hough and Jones, 1997). But in 1992 researchers discovered that the M_w 7.3 Landers, California, earthquake triggered seismicity at much further distances (Hill *et al.*, 1993). Since then, a number of other $M \geq 7$ earthquakes (Brodsky *et al.*, 2000; Glowacka *et al.*, 2002; Prejean *et al.*, 2004; West *et al.*, 2005) as well as smaller M 2–4 mainshocks (Felzer and Brodsky, 2006) have been shown to trigger earthquakes at distances out to tens of mainshock fault lengths. These new observations have generated substantial controversy regarding whether distant triggered earthquakes are regular aftershocks—that is, generated by the same physical process as near-field events—or represent a separate phenomena (Hough, 2005; Steacy *et al.*, 2005; Main, 2006).

One convenient place to investigate the size of the regular aftershock zone is in the Anza, California, region along the San Jacinto fault (Fig. 1). Together the northwest trending San Jacinto and San Andreas faults in southern California accommodate over 80% of right-lateral plate motion (Fay and Humphreys, 2005). The slip rates on the San Jacinto fault are approximately 10 mm/yr (King and Savage, 1983), and the largest earthquakes in this region are typically right-lateral strike slip. The Anza region contains a dense seismic network, ANZA, operated by the Scripps Institution of Oceanography (see the Data and Resources section), in addition to several stations run by the Southern California Seismic Network (SCSN), and has a substantially lower seismic

attenuation than other densely instrumented regions in California. The benefit of data recorded in regions of low attenuation is that a stronger signal reaches the surface, making interpretation of seismograms easier. Anza is characterized by a very competent granitic geology, and despite a number of shallow regions of low Q, Hough *et al.* (1988) found an average Q of ~1000 at seismogenic depths for P and S waves. At Parkfield, on the other hand, another well-instrumented region, Abercrombie (2000) found an average Q of 200 on the southwest side of the fault, an average Q of 100 on the northeast, and a thick layer of lower Q (varying from around 20 to 55) near the surface—a layer so thick, in fact, that the Parkfield borehole stations are deployed within it, not below it.

M_w 5.0 and M_w 5.2 mainshocks occurred in the Anza region in 2001 and 2005, respectively (Fig. 1). For both mainshocks a large number of small aftershocks were recorded, and relatively large aftershock zones were observed. In the case of the 2005 mainshock, aftershocks extended at least 50 km along the San Jacinto fault zone (Fig. 2) (Ⓔ movies of the aftershock sequences are available in the electronic edition of *BSSA*). From the empirical magnitude/fault length relationships of Wells and Coppersmith (1995) we estimate that the 2005 M_w 5.2 mainshock was only ~4.5 km long. Thus the observed 50 km long aftershock zone was viewed by the seismological community as an uncommon occurrence, and it was hypothesized that it was caused by an observed aseismic slip patch that presumably

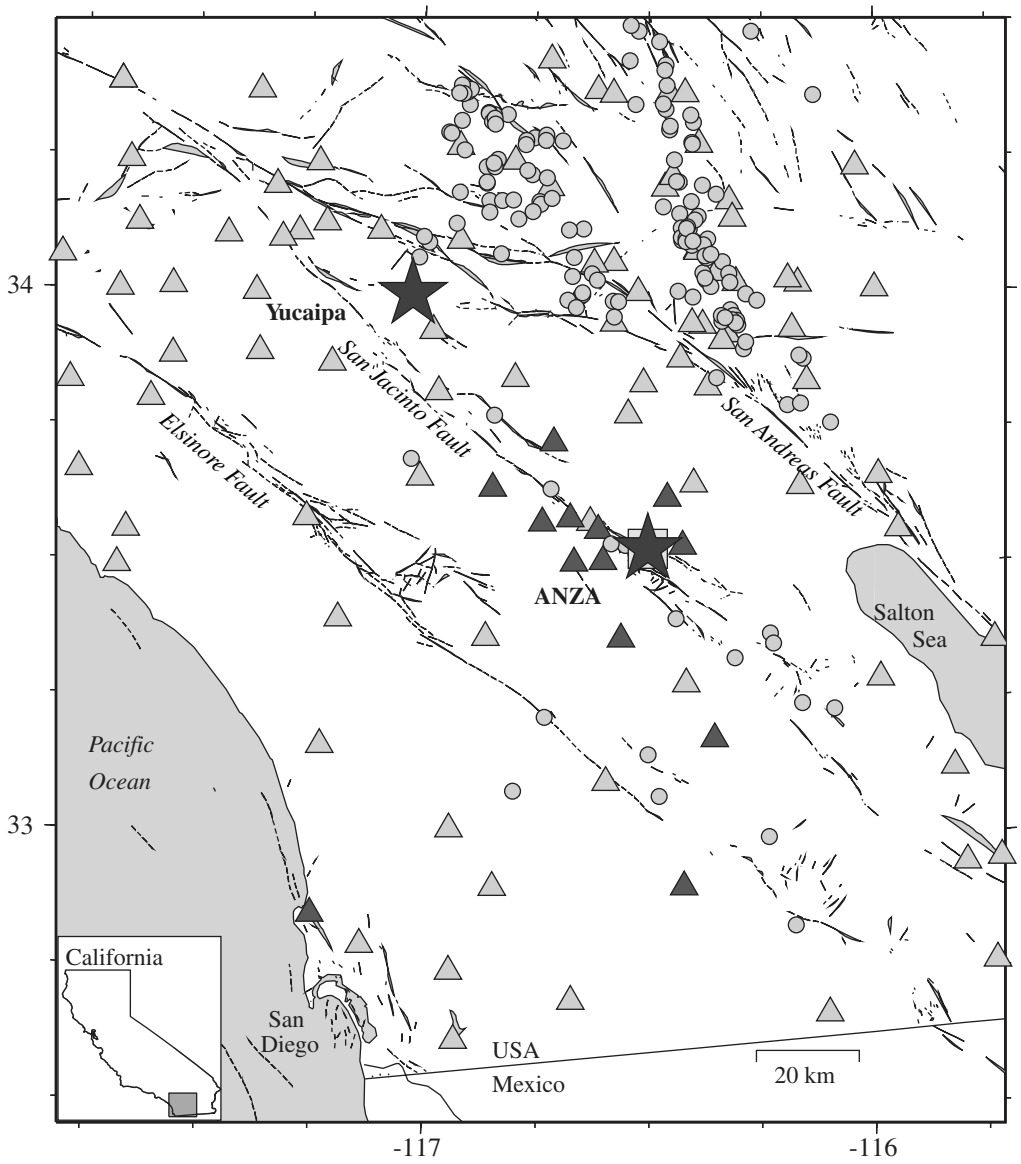

Figure 1. The 2005 M_w 5.2 Anza and 2005 M_w 4.7 Yucaipa earthquakes (labeled with large stars). The 2001 M_w 5.0 Anza mainshock (square) was within ~5 km of the 2005 Anza mainshock. Also shown are the ANZA network stations (black triangles), SCSN stations (gray triangles), 154 $M > 4.0$ events in the region, from the ANZA catalog that occurred during years 1982–2005 (gray circles), and primary fault traces in the southern California region (black lines with major faults labeled).

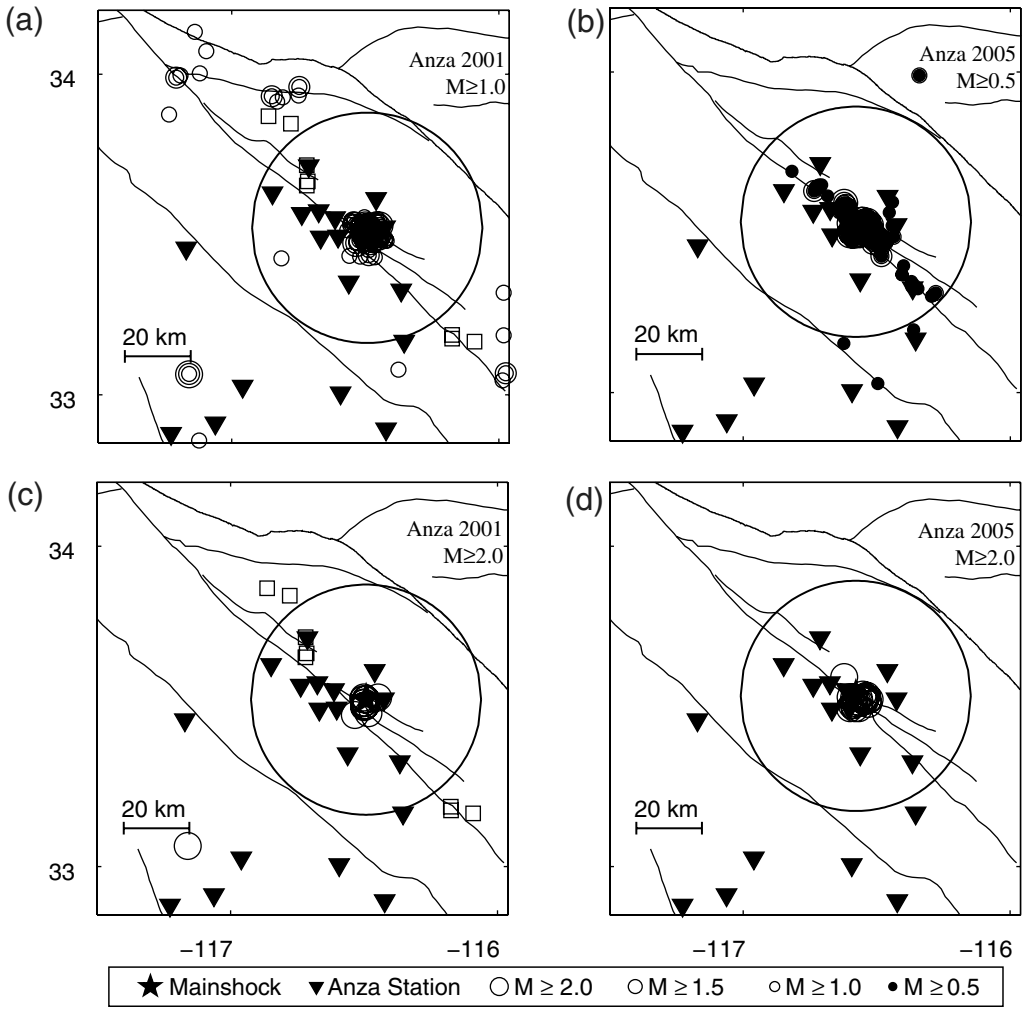

Figure 2. Map of the first 2 days of the aftershocks in the 2001 and 2005 Anza sequences recorded by ANZA seismic network stations (inverted triangles). The top panels plot earthquakes down to the catalog completeness threshold, while the bottom panels plot only those down to M 2, the more common completeness threshold for California aftershock sequences. For reference, a 40 km radius circle is drawn around each mainshock epicenter. Gray lines denote the major faults. (a) The 198 recorded $M \geq 1.0$ aftershocks of Anza 2001. (b) The 387 $M \geq 0.5$ aftershocks of Anza 2005. (c) The 15 $M \geq 2.0$ aftershocks of Anza 2001. (d) The 25 recorded $M \geq 2.0$ earthquakes of Anza 2005. The squares in each figure part depict seismicity in the 2 days before each mainshock, down to the same magnitude cutoffs. There was very little seismicity in the 2 days preceding the 2005 mainshock.

encompassed the region of aftershock activity (Agnew and Wyatt, 2005). The data are not sufficient to determine the exact position or size of this aseismic slipping patch. It is also not known whether large patches of aseismic slip routinely accompany earthquakes because the strainmeter instrumentation needed to record these phenomena is not commonly used and was not even operational during the 2001 Anza mainshock/aftershock sequence.

In this article, we demonstrate that the large extent of the 2005 Anza aftershock sequence was not likely caused by an unusual aseismic event. This conclusion is based on our observation that the density of aftershocks decayed with distance from the mainshock fault at the same rate as observed elsewhere in California. This typical decay was also seen after the 2001 Anza sequence. Furthermore, both Anza sequences agree well visually with simulations of normal aftershock sequences with low earthquake catalog completeness levels. This suggests that if we could routinely catalog many small aftershocks, most aftershock zones would appear to cover a wide area. We also demonstrate that despite the large aftershock zones of the Anza earthquakes, the M_w 4.9 earthquake near the town of Yucaipa, which occurred 4 days after and 72 km away from the 2005 Anza mainshock, was probably not triggered by this event.

Data

We examine the mainshock and aftershock sequences of the 31 October 2001 M_w 5.0 Anza earthquake (33.52°, −116.50°, depth 18 km) and 12 June 2005 Anza M_w 5.2 earthquake (33.53°, 116.58°, depth 14 km). We also look at the relationship between the 2005 Anza mainshock and

the M_w 4.9 Yucaipa earthquake (33.99°, −117.03°, depth 17 km) that occurred 4 days later. The two Anza sequences occurred directly under the ANZA seismic network (see the Data and Resources section), which spans the San Jacinto fault zone in southern California (Berger *et al.*, 1984; Vernon, 1989). Rarely are continuous waveform data of such high quality available. Within our local study region (32.0° < latitude < 34.5°, −117.90° < longitude < −115.60°, depth < 25 km) the Anza network catalog contains 499 and 1615 earthquakes in the initial two days for the 2001 and 2005 sequences, respectively (Fig. 3).

We augment the 2005 ANZA network data with data from the SCSN catalog (see the Data and Resources section). We quantify the degree of variability between the ANZA and SCSN catalogs by comparing 881 earthquakes common to both catalogs (350 in the 2001 sequence and 531 in the 2005 sequence). The mapped (i.e., latitude and longitude) location differences between the two networks are 1.1 and 1.9 km for the 2001 and 2005 data, respectively, and the ANZA network reports that the earthquakes are deeper on average by approximately 2–3 km. The depth differences between the SCSN and ANZA catalogs could be a result of the use of different velocity models. The SCSN location algorithm uses a model based on Hadley and Kanamori (1979) (D. Given, personal comm., 2009) while the ANZA algorithm uses the IASPEI91 model (F. Vernon, personal comm., 2009). The magnitudes of the two earthquake catalogs (i.e., ANZA and SCSN) also differ. The median difference in the assigned magnitudes is about 0.5 ± 0.3, with earthquakes in the SCSN catalog on average ~0.5 magnitude units higher than the corresponding earthquake in the ANZA network catalog, although with significant scatter (Fig. 4). The discrepancy in magnitudes likely arises from a combination of different station corrections used by the two networks and the fact that the primary footprint of the ANZA network spans a relatively small area (F. Vernon, personal comm., 2009). These data have hypocentral distances of <20 km, and short hypocentral distances have been shown to bias magnitudes downward (Bakun and Joyner, 1984).

Method

Investigating the Large Spatial Extent of the Anza Aftershock Sequences

The first question we address is whether the spatially extended 2005 Anza aftershock sequence comprises normal, seismically triggered aftershocks or seismicity triggered by some other mechanism such as a zone of extended aseismic slip. We do this by measuring how quickly the density of triggered aftershocks decays with distance from the mainshock fault plane and visually comparing the sequence with simulated ones that follow typical aftershock statistics. Included in our simulation is a low aftershock magnitude detection threshold comparable to the one attained by the ANZA network. Using this approach we are assuming that aseismic slip patches do not routinely accompany $M \sim 5$ earthquakes.

Felzer and Brodsky (2006) derived that for southern California aftershock sequences aftershock density decays on average with distance, r, as

$$\rho(r) = cr^{-1.37}, \tag{1}$$

where r is the shortest distance, in 3D, between the aftershock and the mainshock fault plane, and $\rho(r)$ is linear density, which measures the number of aftershocks per kilometer. The constant c gives the total aftershock productivity and, thus, is a function of the modified Omori law parameters (see

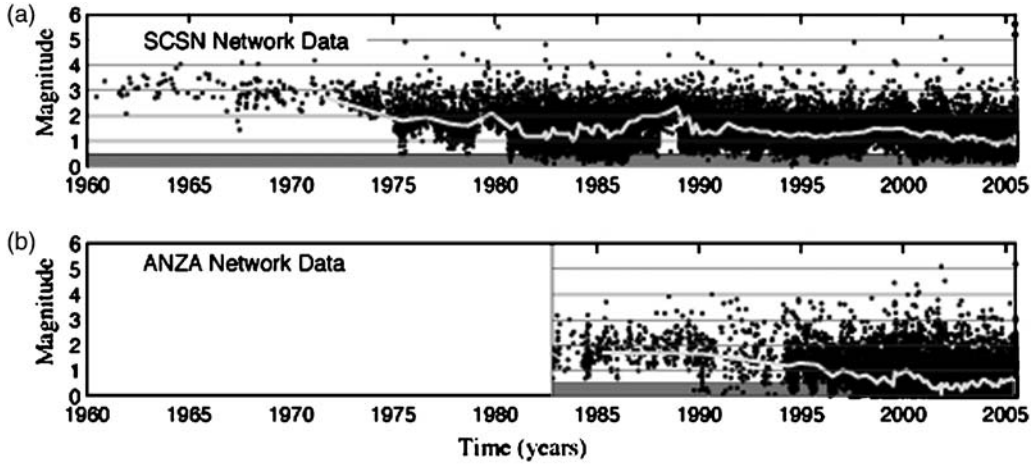

Figure 3. Temporal examination of earthquake magnitudes (points) recorded by the SCSN and ANZA networks. Data are restricted to the region 33.3° < latitude < 33.75° and −117.25° < longitude < −116.25°. This region was chosen to be as big as possible while at the same time avoiding the large signature of the M_w 7.3 1992 Landers earthquake and the M_w 7.1 1999 Hector Mine earthquake. Only recently have small magnitude earthquakes been routinely recorded and cataloged, as indicated by the decrease in the median earthquake magnitude for a moving window of 250 consecutive events (nonlinear gray line). For reference, the shaded region encompasses magnitudes below 0.5. (a) SCSN data (35,293 earthquakes); (b) ANZA data (23,922 earthquakes).

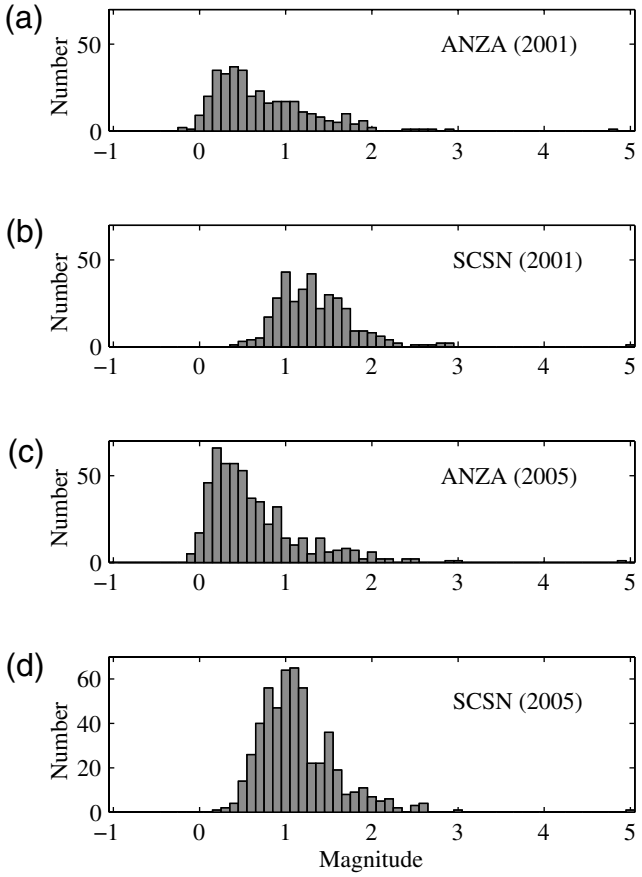

Figure 4. Comparison of earthquake magnitudes for common event pairs in the ANZA and SCSN catalogs. Data consist of 350 and 531 earthquake pairs in the 2001 and 2005 sequences, respectively. The mean difference in magnitudes for the 2001 sequence is 0.6 ± 0.3 and for the 2005 sequence is 0.5 ± 0.3. (a) Magnitude histogram of data from the ANZA network catalog for the 2001 sequence. (b) as in (a) but for the SCSN catalog. (c) Magnitude histogram of data from the ANZA network catalog for the 2005 sequences. (d) As in (c) but for the SCSN catalog.

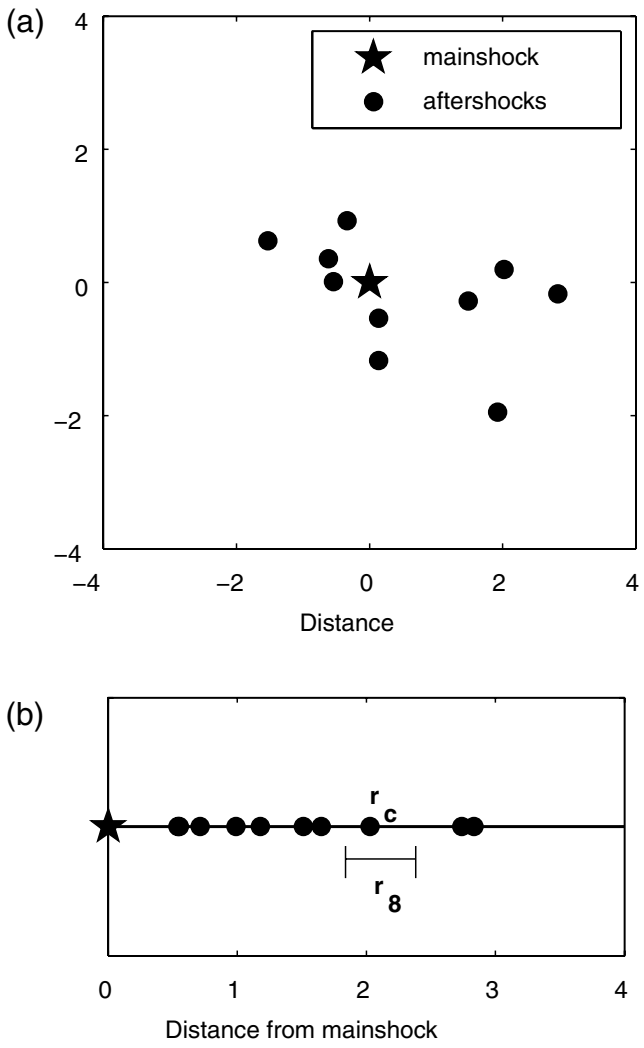

Figure 5. Schematic of measuring linear aftershock density with the nearest neighbor technique, with k (number of earthquakes/group) set equal to 1. Distance units are generic and therefore not included because this figure merely illustrates our measurement method. (a) A mainshock and ten aftershocks are plotted in map view. (b) The aftershocks are depicted on a line where their position is dictated by their distance from the mainshock. As an example, we calculate linear density at the position of the eighth aftershock. Because the earthquake group size is 1, the center point of the measurement, or r_c, is at the position of this aftershock. Linear density at r_c is given by k/r_8 or $1/r_8$, where r_8 reaches from the midpoint between aftershocks 7 and 8 to the midpoint between aftershocks 8 and 9.

the Appendix) and mainshock magnitude. Aftershock decay at Anza may be considered normal if it agrees well with equation (1), which we determine using three different tests.

As a first test we fit the linear density of the Anza aftershocks as a function of distance. The linear density is measured with the nonparametric nearest neighbor method (Silverman, 1986). In this method the aftershocks are first plotted on a line as a function of their distance, r, to the mainshock fault (Fig. 5). Consecutive points on the line are then placed into groups, with the same number of aftershocks in each group. The density at the center of each group, at distance r_c from the mainshock, is given by

$$\rho(r_c) = \frac{k}{r_n}, \tag{2}$$

where k is equal to the number of points in each group and r_n is the length of the nth group, as illustrated in Figure 5.

We use $k = 1$, which maximizes the data scatter but gives us the lowest parameter fitting error because smoothing, and information loss, is minimized. The azimuth of the aftershocks is not used in the calculation of linear density and does not affect the results.

Second, as a more quantitative version of the first test, we count the number of earthquakes in annuli around the 2001 and 2005 Anza mainshocks and compare these values with predictions from equation (1). Details are given in the Results section.

Finally, we do a visual comparison of the Anza aftershock sequences with simulations produced with the epidemic type aftershock sequence (ETAS) aftershock model (Ogata, 1988; Felzer *et al.*, 2002; Helmstetter *et al.*, 2006). The ETAS model simulates aftershocks using robust empirical laws of aftershock behavior. The laws we use are the modified Omori law for aftershock rate decay with time (Utsu, 1961) (see the Appendix for the calculation of our modified Omori law parameters), the Gutenberg–Richter magnitude–frequency relationship (Gutenberg and Richter, 1944), and the Felzer–Brodsky relationship (Felzer and Brodsky, 2006) (equation 1) for the decay of aftershock density with distance. A b-value of 1.0 is used for the Gutenberg–Richter relationship as this is the value found in the vast majority of California (Felzer, 2006) and is consistent with what we see at Anza. Specific b-values calculated at Anza, using the completeness magnitudes for each sequence as specified subsequently, are 1.07 ± 0.18 and 1.37 ± 0.27 for the 2001 sequence with magnitudes taken from the ANZA and SCSN catalogs, respectively (errors calculated at the 98% confidence level with the maximum likelihood equation of Aki [1965]), and 0.81 ± 0.1 and 1.14 ± 0.14 for the 2005 sequence using magnitudes from the ANZA and SCSN catalogs, respectively. The variability in calculated b-values likely results from the uncertainty in Anza magnitudes as discussed previously. The largest aftershock we allow in the simulation is M 3.65, which is the magnitude of the largest earthquake in the data catalog for this region. Using the maximum magnitude in the real data for the simulation is important because the overall productivity of the aftershock sequence will vary with the largest aftershock magnitude, and the apparent spatial extent of the aftershock sequence, in turn, varies with this overall productivity.

We inspect only the first two days of aftershocks for both the 2001 and 2005 sequences because this time period is short enough to minimize the inclusion of unrelated background earthquakes while being long enough to provide a reasonable amount of aftershock data. Because we use data down to small magnitudes and over a large area, the background earthquakes can accumulate quickly, so a short time period for measuring aftershocks is essential.

An important issue for all of our tests is catalog completeness. When we measure the decay of aftershock density with distance we do not need our catalog to be 100% complete above our chosen magnitude threshold, but we do need the level of completeness to be consistent over the distance range inspected. We test for completeness consistency by measuring the correlation coefficient between distance from the mainshock and the magnitudes of aftershocks in the ANZA catalog. When the catalog is limited to $M \geq 0.5$ earthquakes, we find no significant correlation for distances ranging up to 40 km. Beyond 40 km, the correlation becomes positive, presumably because we are leaving the core of the Anza network. Thus for our quantitative measurements of aftershock density as a function of mainshock–aftershock distance (our second test) we limit our data to $M \geq 0.5$ earthquakes located at 40 km or less from the mainshock fault plane.

For our qualitative comparison between the 2001 and 2005 Anza aftershock sequences and the ETAS simulation (our third test) of these sequences we need an estimate of the absolute completeness threshold, which will serve as the minimum magnitude for our simulations. Determining the absolute completeness threshold is a very difficult task. The most comprehensive method is to invert for the detection sensitivity of nearby seismic stations and then forward-solve for the completeness at each point given its distance from each station (Schorlemmer *et al.*, 2006). This method is complex, however, and our current problem does not require such an accurate solution. So instead, we solve for completeness with magnitude–frequency plots of the data, qualitatively estimating at what magnitude the number of earthquakes falls below that predicted by the Gutenberg–Richter magnitude–frequency relationship (Gutenberg and Richter, 1944). This method yields completeness thresholds of $M \sim 1.5$ and $M \sim 1.0$ for the 2001 Anza sequence in the SCSN catalog and ANZA network catalogs, respectively. For the 2005 Anza sequence the fall-off occurs at $M \sim 1.0$ in the SCSN catalog (Fig. 6). A fall-off is not readily apparent in the 2005 ANZA network catalog for magnitudes down to M 0. Because we previously found evidence that the Anza catalog becomes incomplete below M 0.5 near the edges of the Anza region we assign a threshold of M 0.5 for this catalog.

Another concern with our data is potential inaccuracy in the calculated distances between the aftershocks and the mainshock fault plane in the near field, caused by errors in aftershock locations and our assumption that the 2001 and 2005 Anza mainshocks ruptured perfectly planar faults. Most large earthquake rupture planes have complexities, such as irregular fault surfaces, stepovers, and bends. A study by Walker *et al.* (2005) found aftershocks in the 2001 Anza sequence to be quite heterogeneous (41% strike slip, 41% thrust, and 18% normal based on earthquakes in the first month of the sequence), suggesting that this mainshock fault surface was particularly complex. To avoid this near-field complexity we do not use aftershocks that are closer than 4 km to the modeled position of the mainshock fault plane in our quantitative analysis. The 4 km limit is approximately the average fault length of our mainshocks.

Our distance, time, and magnitude cutoff requirements as specified previously result in a total of 68 aftershocks for quantitative analysis of the 2001 Anza sequence using the ANZA catalog, a total of 49 aftershocks for analysis of the 2005 Anza sequence from the ANZA catalog, and a total of 55 aftershocks for our quantitative analysis of the 2005 sequence using the SCSN catalog. We do not use 2001 SCSN data in our analysis because of the paucity of data in this catalog, which is in part because ANZA station recordings were not incorporated into the SCSN earthquake location routines at that time. For the qualitative comparison of map views of the data with map views of the simulations,

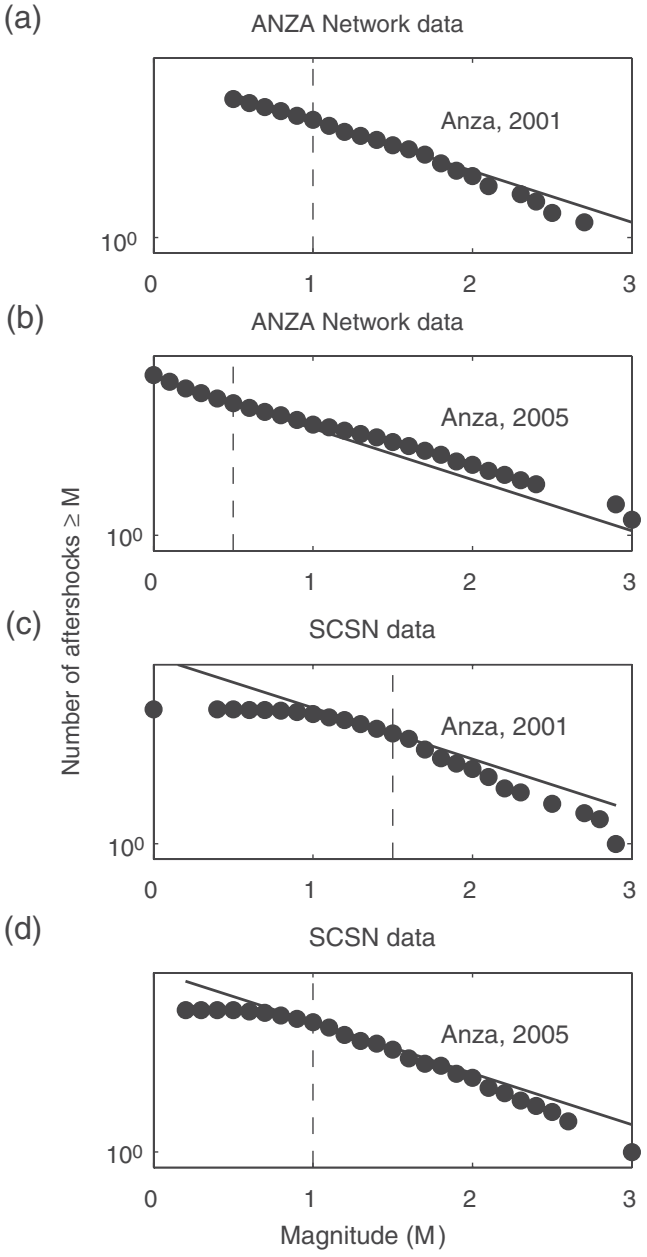

Figure 6. Cumulative magnitude–frequency plots of the first 2 days of aftershocks in the 2001 and 2005 Anza sequences, used to roughly estimate sequence magnitude completeness thresholds (m_c). The Gutenberg–Richter relationship with $b = 1$ is included with each plot (solid line) along with the estimated completeness threshold (dashed line). For these cumulative frequency plots the completeness threshold is 0.3–0.4 magnitude units above where the data visually deflect from the Gutenberg–Richter line. (a) 2001 sequence from the ANZA network (499 aftershocks, m_c 1.0). (b) 2005 sequence from ANZA network (1351 aftershocks, m_c 0.5). (c) 2001 sequence from the SCSN network (421 aftershocks, m_c 1.5). (d) 2005 sequence from the SCSN network (593 aftershocks, m_c 1.0).

for which we cover distances from 0 to 100 km, we have 198 $M \geq 1.0$ aftershocks in the first 2 days of the 2001 ANZA network catalog and 387 $M \geq 0.5$ aftershocks in the first 2 days of the 2005 ANZA network catalog.

Investigating Whether the Yucaipa Earthquake Was Triggered by the 2005 Anza Mainshock

Given the proximity in space and time between the 2005 Anza and Yucaipa earthquakes (4.2 days and 72 km), and the broad region covered by the 2005 Anza aftershocks, we investigate the probability that the Anza mainshock triggered the earthquake in Yucaipa. A direct solution would require knowing what the seismicity rate would have been in the absence of the Anza mainshock at the point and time where the Yucaipa earthquake nucleated. Answering this question precisely is extremely complex in part because it requires accounting for all previous aftershock sequences that could possibly affect the region, including sequences triggered by mainshocks too old, distant, or small to be in the catalog. The vulnerability to triggering of the Yucaipa epicentral region at the time that the 2005 Anza earthquake occurred also needs to be known. Because there are too many unknowns for such a precise calculation, we compute instead a general empirical solution of the probability that an M 5–6 mainshock in California will trigger an $M \geq 4$ earthquake at 4.2 days and 72 km. We use M 4.0 as our cutoff to look for triggered earthquakes rather than M 4.9 because this lower threshold increases the potentially detected triggered earthquakes by tenfold. Repeated study has shown that aftershocks follow the Gutenberg–Richter magnitude–frequency relationship, and thus if $M \geq 4$ aftershocks occur then so will $M \geq 4.9$, just at roughly one tenth the rate (Felzer *et al.*, 2004). This general calculation has the benefit of being applicable to other triggering scenarios, but the disadvantage that we do not know to what extent vulnerability to triggering at Yucaipa is similar to the rest of the state. Given that the Yucaipa area does not regularly experience either unusually high or low aftershock activity after local mainshocks, however, we feel that it is reasonable to assume that the local sensitivity to triggering is not sharply different than elsewhere.

To compute this empirical triggering probability we first select all M 5–6 earthquakes from the SCSN and the Advanced National Seismic System (ANSS) catalogs occurring in California from 1984–2006 that were not preceded within $T1$ days by a larger earthquake anywhere in the state. The year 1984 is chosen as a starting point because after this date a good, statewide, instrumental earthquake catalog exists. The exclusion of larger earthquakes for $T1$ days is done so that the resulting catalog will contain earthquakes that are much more likely to be triggered by the selected mainshocks than by some other larger earthquake. We next chose an earthquake triggering inspection time, $T2$. Finally, the background seismicity rate is estimated from seismicity occurring from time $-T3$ to -0.5 days before each select mainshock. Seismicity occurring in the last 0.5 days before the mainshock is not included because the seismicity rate can be strongly increased by foreshock activity right before the mainshocks. Because it is impossible to remove aftershocks of foreshocks from the data, technically the triggered earthquakes that we observe could have been triggered by either the target

mainshocks or by foreshocks that preceded the mainshocks within 12 hr.

We find that the background rate changes by about a factor of 2 when $T1$ is varied between 50 and 500 days, where background earthquakes are defined as all seismicity not triggered by the target M 5–6 mainshocks. Higher background rates are seen for smaller values of $T1$ and lower background rates for larger values, presumably because aftershock production by the bigger earthquakes continuously decreases with time. Statewide background rates for various values of $T1$ are given in Table 1. Because increasing $T1$ decreases background rates, larger values of $T1$ allow small triggering rates to be seen more easily and at higher confidence. Increasing $T1$ also decreases the available number of target mainshocks, however, increasing the variability of the measured triggering rate and ultimately leaving too few mainshocks for triggering to be seen at all. Therefore, we calculate the fraction of distant earthquakes that are triggered for M 5–6 mainshock data sets corresponding to a range of values of $T1$ between 50 and 500 days (Table 1). The larger values allow us to demonstrate that some triggering is indeed occurring, while the full range of values helps us to constrain what that rate of triggering is. Values of $T1$ larger than 500 days result in too few target mainshocks to calculate statistics.

We find that the measured background rate is fairly stable for choices of $T3$ (the time at which we start measuring background earthquakes) ranging from 25 to about 75 days (unless $T1 < 75$, in which case the range of stability is narrower). For example, the 2005 Anza mainshock occurred 257 days after the last $M \geq 5.2$ earthquake in California. Setting $T1 = 257$ days and allowing $T3$ to vary from 25 to 75 days, we recover a mean background rate of 0.0285 $M \geq 4$ earthquakes/day with 98% of the values falling from 0.0255 to 0.0293 $M \geq 4$ earthquakes/day. Values of $T3$ shorter than 25 days or longer than 75 days result in higher background rates; in the first case because the rate becomes too dominated by foreshock activity, and in the second case because we start capturing too many aftershocks of the larger mainshocks that occurred prior to $T1$.

Solving for the fraction of earthquakes at ≥ 72 km that are triggered is then done by simply subtracting the calculated background earthquake rate from the total rate observed in the triggering inspection time $T2$ and then dividing by this total as follows,

$$P = (Tot - B)/Tot, \tag{3}$$

where P is the percentage triggered, Tot is the total number of earthquakes observed, and B is the calculated background rate. As demonstrated previously the average value of B is generally quite stable if we use inspection time periods of 25–75 days and a constant value of $T1$. The exact integer number of background earthquakes that may occur on the day of potential triggered earthquakes, however, is of course subject to random Poissonian variation. Therefore, the confidence interval of P is estimated by replacing B with the smallest and largest integer number of background earthquakes that may randomly occur during the time period that triggers are being searched for, at 98% confidence, according to the Poissonian distribution. These confidence intervals are also given in Table 1.

Results

Aftershocks of the Anza Earthquakes

We find that aftershock density as a function of distance from the mainshock for both Anza mainshocks follows an

Table 1

Observed Background Seismicity and Triggering Rates of $M \geq 4.0$ Earthquakes Associated with M 5–6 Mainshocks in California at Distances of > 72 km from the Mainshock Epicenter

$T1$*	N_{main}†	Background Rate‡	Total Rate§, d 0–0.5	Fraction Triggered‖, d 0–0.5	Fraction Triggered‖, d 0.25–0.75
50	67	0.017	0.075	0.77, 0.2–1.0	0.71, 0–1
150	39	0.013	0.10	0.87, 0.5–1.0	0.74, 0–1
257	16	0.012	0.19	0.93, 0.67–1.0	0.89, 0.5–1.0
300	14	0.008	0.21	0.97, 0.67–1.0	0.95, 0.5–1.0
400	11	0.010	0.27	0.97, 0.67–1.0	0.95, 0.5–1.0
500	7	0.009	0.14	0.94, 0–1.0	0.97, 0.5–1.0

M 5–6 earthquakes are chosen as target mainshocks if they are not preceded by a larger earthquake within $T1$ days anywhere in the state. As $T1$ increases the average background seismicity rate (defined as all earthquakes not aftershocks of the target earthquakes) decreases, making triggering easier to detect, but the total number of target mainshocks also decreases.

*$T1$, the minimum number of days between a larger earthquake and a target mainshock.

†N_{main}, number of target mainshocks.

‡Background rate is the average rate of $M \geq 4$ earthquakes/half day from -25 to -0.5 days from the mainshocks over the whole state, excluding a 72 km radius around each mainshock.

§Total rate of $M \geq 4$ earthquakes/half day observed over 0–0.5 days after the target mainshocks over the same area as the background rate.

‖Fraction of $M \geq 4$ earthquakes at ≥ 72 km distance observed to be triggered by the target mainshocks over 0–0.5 and 0.25–0.75 days after the mainshocks. Ranges gives the 98% confidence interval based on the assumed Poissonian variability of the background rate (see text).

inverse power law decay, with decay rates a bit steeper than the California average (Fig. 7). Specifically, while the average power law exponent for southern California is −1.37, the power law exponents measured for the 2001 and 2005 sequences are -1.76 ± 0.14 and -1.85 ± 0.15, respectively, where we give standard errors calculated from 1000 bootstrap regressions. The power law exponent for aftershock density decay is expected to vary somewhat from place to place as a function of fault geometry and perhaps local attenuation relationships. Because the southern California region encompasses so many different types of complex faulting regimes, it is not surprising that the decay rates we derive for the 2001 and 2005 sequences are not exactly the same as the southern California average. What is significant is that both sequences give approximately similar decay rate estimates and that these estimates are consistent with the rates found in other parts of California. In northern California, for example, the average exponent is −1.8 (Felzer and Brodsky, 2006). The most important point for our purposes is that the distribution of Anza aftershocks is similar to those observed in other, assumed typical, aftershock sequences. We conclude that there is no excess aftershock activity at distances that would indicate the need for an unusual triggering mechanisms such as an aseismic slip patch.

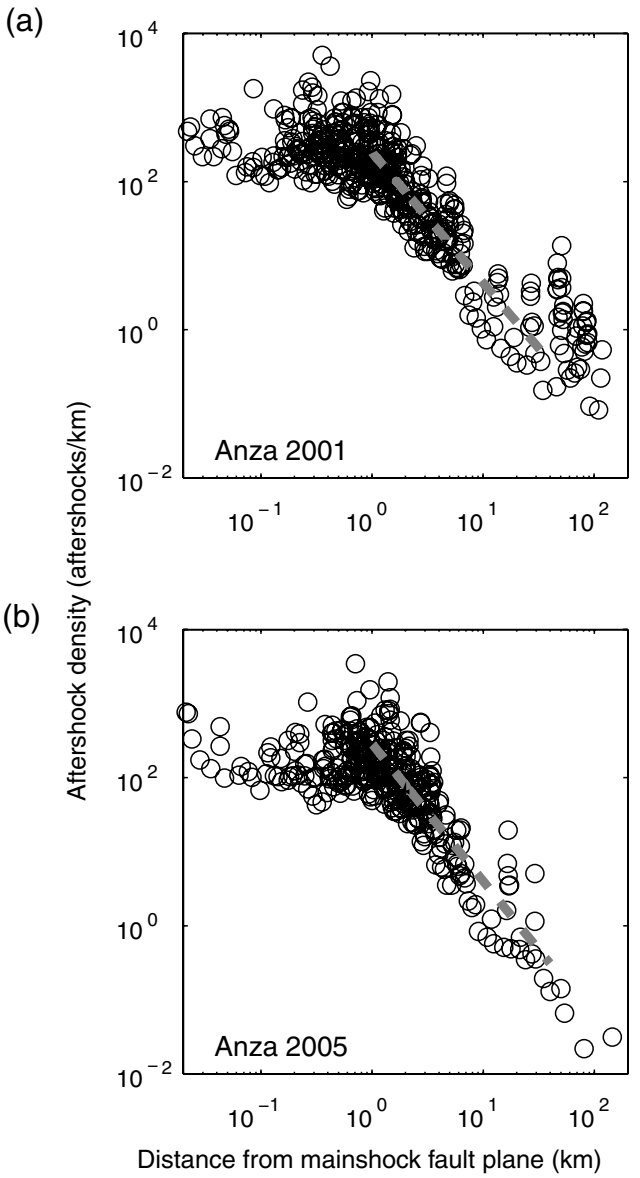

Figure 7. Aftershock hypocentral distance from the mainshock versus aftershock density, restricted to $M_L \geq 0.5$ ANZA network data (open circles). Aftershock data points that locate between 4 and 40 km from the mainshock are used to determine a best-fit distance-to-density relationship (dashed gray line) and associated decay values. These lines are then extrapolated to a 1 km distance for visual comparison. At very close distances we expect the decay curve to flatten because of earthquake mislocation, inaccuracies of the modeled mainshock fault plane, and near-field catalog incompleteness (e.g., see Felzer and Brodsky, 2006) (a) The 68 aftershocks in the 2001 Anza sequence have a best-fit exponent of −1.76. (b) The 49 aftershocks in the 2005 Anza sequence have a best-fit exponent of −1.85.

We next confirm that the decay of aftershock density with distance for the Anza sequences is normal by breaking the distance from 4 to 40 km from the mainshocks into successive annuli of 6 km width and counting the number of earthquakes in each annulus. The mean number of earthquakes that we expect in each annulus is given by equation (1), where the constant c in that equation is determined from the total number of aftershocks observed in the annulus stretching from 4 to 10 km. For the ANZA catalog of the 2001 and 2005 sequences, this gives c values of 366 and 230 for $M \geq 0.5$ aftershocks, respectively. For the SCSN 2005 earthquake catalog, a c value of 270 is found for $M \geq 1.0$ aftershocks. The 98% range on the number of earthquakes that we expect to observe in each annulus, given data set size, is calculated via 500 ETAS simulations. We find that the 16–22 km distance bin for the 2001 sequence has fewer aftershocks than expected, falling below the 98% confidence interval of the model, but the number of aftershocks within the rest of the annuli for both the 2001 and 2005 sequences are within the expected ranges (Fig. 8). Despite the fact that the data fit within the model 98% confidence intervals, the majority of points are below the predicted mean. Presumably this is because the actual decay of aftershock density with distance at Anza follows a steeper power law than the California average, as discussed previously.

As a final test, we qualitatively compare map views of the 2001 and 2005 Anza aftershock sequences with random realizations of our ETAS simulated aftershock sequences (Fig. 9). We conclude that the data are consistent with the simulations. While only a single random simulation is presented in these maps, the error bars in Figure 8 describe the spread of 500 calculations of each sequence and show that the simulated results encompass the real data. These models demonstrate that when aftershock sequences following the statistical empirical ETAS model laws are visualized using aftershocks as small as M 0.5 or M 1, the spatial distribution appears much larger than if only using aftershocks $M \geq 2.0$, which is the more common completeness threshold in California data.

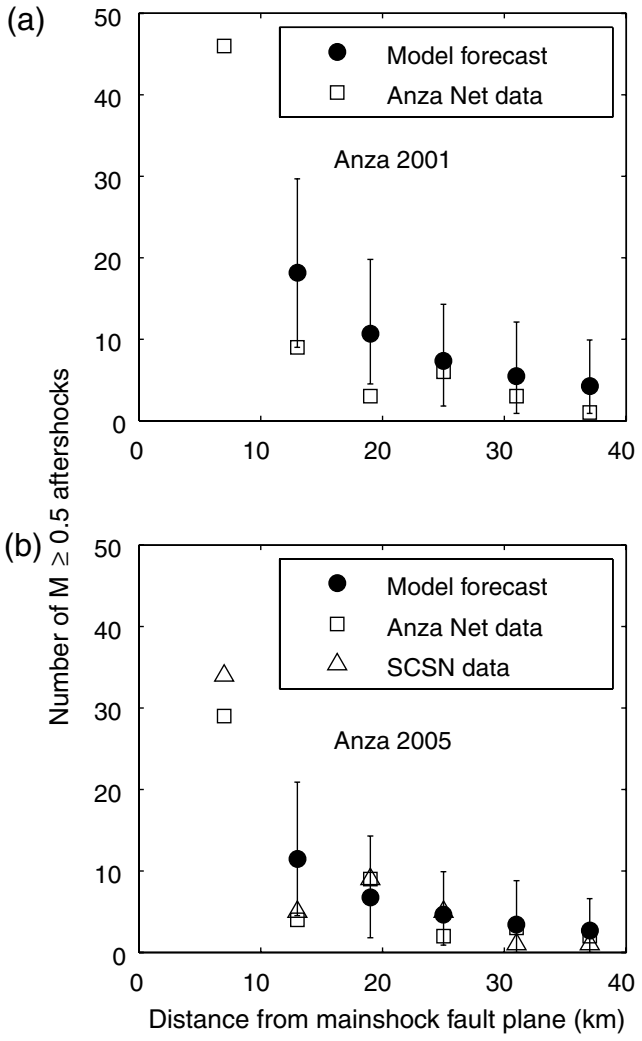

Figure 8. Expected (solid symbols) and observed (open symbols) number of aftershocks (restricted to $M_L \geq 0.5$) in the first 2 days of each sequence as a function of distance between the aftershock hypocenter and mainshock fault plane for the (a) 2001 Anza sequence and (b) 2005 Anza sequence. The expected number of aftershocks in distance bins that range between 10 and 40 km are extrapolated using the number of observed aftershocks between 4 and 10 km and equation (1). Error bars give the 98% confidence range of the modeled values, estimated from 500 ETAS simulations with data sets of this size. The observed number of aftershocks from the ANZA network catalog (squares) and the observed number in the SCSN catalog (triangles) primarily fall within the modeled error bars. Because there is a 0.5 magnitude unit offset in the ANZA and SCSN catalogs, for the SCSN data we only measure $M \geq 1.0$ earthquakes.

Triggering of the Yucaipa Earthquake

We next investigate if the 2005 Anza mainshock triggered the 2005 Yucaipa earthquake that occurred 4.2 days later and 72 km away. Over the last 60 yr there has been an average of 3.6 $M \geq 4.9$ earthquakes (including all aftershock sequences) recorded per year in our southern California study region. (Note that most of the southern California catalog is complete to M 4.2 from 1932 on [Felzer, 2008].) The exceptions are the first day of the aftershock sequence of the 1992 M 7.3 Landers earthquake, which is complete to M 4.7 after the first 5 min (Helmstetter *et al.*, 2005), and the aftershock sequence of the 1952 M 7.5 Kern County earthquake, which we estimate is complete to M 4.6–4.7 by comparison with the Gutenberg–Richter magnitude–frequency relationship. Thus if we were to assume a stationary seismicity rate, the probability of randomly having two $M \geq 4.9$ earthquakes separated by 4 days or less is only ~3%.

We estimate, as described in equation (3), the probability that the Yucaipa earthquake was triggered by the Anza earthquake by looking at triggering, at distances up to 72 km, of $M \geq 4$ earthquakes surrounding M 5–6 mainshocks throughout the state of California. Our catalog, generated by the Working Group on California Earthquake Probabilities (WGCEP) (Felzer and Cao, 2008), includes earthquakes from California and regions within 100 km of the state border, which occurred between 1984–2006. We assume that the 72 km distance between the Anza and Yucaipa mainshocks is in error by less than 2 km, consistent with location error in the rest of the southern California catalog, and so no other distance ranges are tested.

The first important result is that we can observe clear triggering (> 98% confidence) by the M 5–6 mainshocks at distances of > 72 km for short time periods after the mainshocks (Table 1), even though 72 km is more than ~5 times longer than the fault length of our largest mainshock. Within 0.5 days of the mainshock, for example, the rate of earthquakes is 4–16 times the background (Table 1). The existence of triggering at > 72 km can also be seen at 98% confidence at time intervals of 0.25–0.75 days.

Triggering cannot be verified with high confidence for an inspection time, $T2$, of 0.5–1.0 days, or any later time period regardless of the choice made for $T1$. This may be because triggering stops sometime between 0.5 and 0.75 days, and if so the Yucaipa earthquake could not have been triggered by the 2005 Anza mainshock. Alternatively, triggering may continue beyond 0.5 days but at such a low rate it cannot be detected above the background at high statistical confidence. For example, if the Poissonian distribution of the background rate indicates we should expect between $B1$ and $B2$ background earthquakes, then we need to observe more than $B2$ earthquakes in order for our results to be statistically significant. If the triggering rate shows that $>(B2 - B1)$ triggered earthquakes can be reliably expected, yet $> B2$ earthquakes are not observed, then we can conclude that triggering is absent. On the other hand if fewer than $B2$ earthquakes are observed but the expected number of triggered earthquakes is $\leq(B2 - B1)$, it is possible that triggering continues, but it is obscured by the low signal-to-noise ratio. This is a reasonable assumption given that triggering is observed to continue after 0.5 days at closer distances.

As a first step we find what the aftershock rate should be at 72 km and 0.5–1 days by extrapolating the triggering rate observed at 0.25–0.75 days using Omori's law for aftershock decay (Omori, 1894),

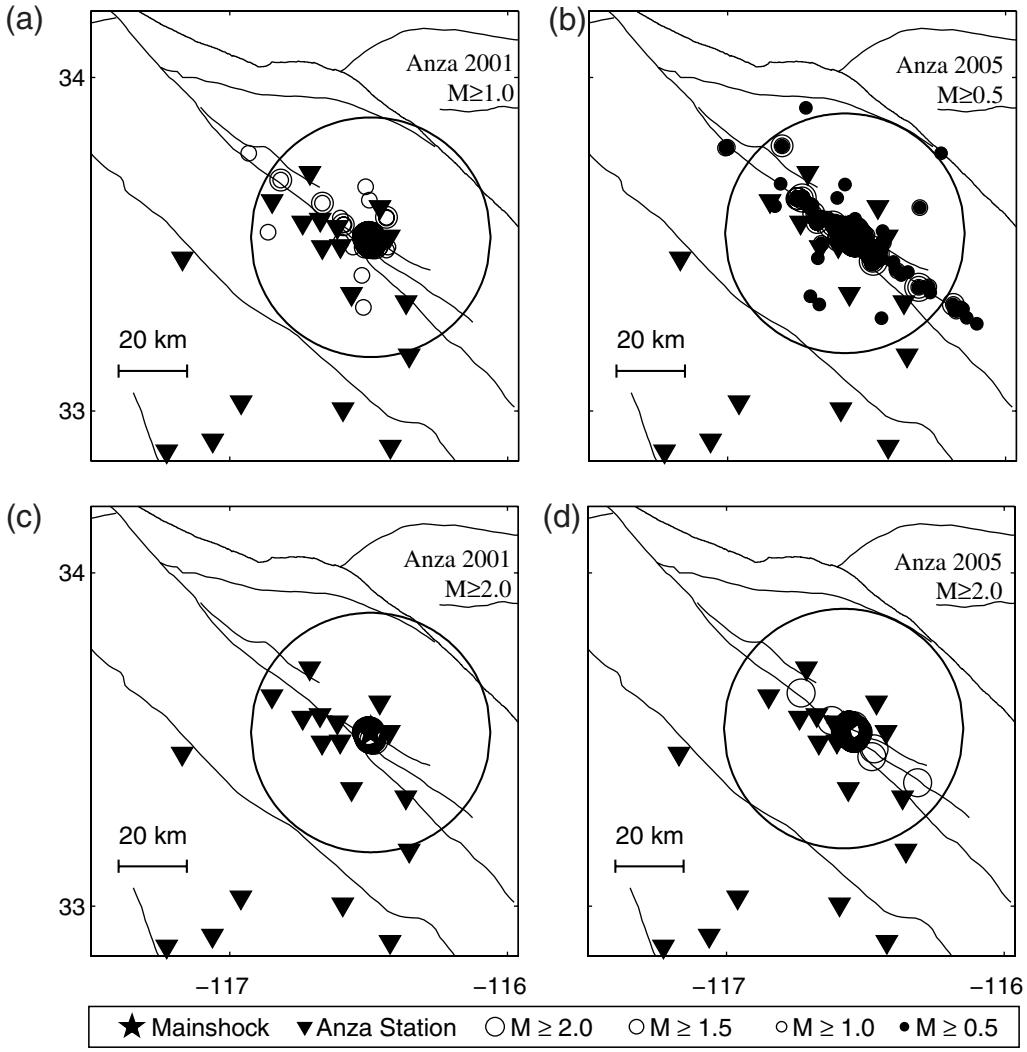

Figure 9. Simulation of the first 2 days of aftershocks in the 2001 and 2005 Anza sequences. These maps can be compared with the real data in Figure 2. For spatial reference, a 40 km radius circle is drawn around each mainshock epicenter. These maps illustrate, even in the simulations, how much smaller the sequences appear when only aftershocks larger than magnitude 2, the usual completeness threshold for southern California aftershock sequences, are plotted. Data from simulations of (a) the 2001 Anza sequence for 348 $M \geq 1.0$ earthquakes and (b) the 2005 Anza sequence for 1585 $M \geq 0.5$ earthquakes. (c) As in (a) but including only the 49 $M \geq 2.0$ earthquakes, and (d) as in (b) but including only the 40 $M \geq 2.0$ earthquakes. While only single simulated sequences are plotted here, the range of aftershock densities at different distances from a total of 500 ETAS simulations are plotted in Figure 8. Although the numbers of aftershocks given in (a)–(d) are all greater than that observed in the real sequences, Figure 8 indicates that the range of simulation results encompasses the real data.

$$r = Kt^{-p}, \tag{4}$$

where r is the aftershock rate, t is time, and K and p are constants. Here we do not include the c value used in the modified Omori law $(K(t+c)^{-p})$ (Utsu, 1961) because the c value is generally small ($\ll 1$ day) and thus unimportant at later times. We also do not have enough data to solve for the value of p, so we set it at the average California value of 1.08 found by Reasenberg and Jones (1989). We then find the full range of possible values of K by setting $T1$, or the exclusion period for larger earthquakes, at values varying between 50 and 500. Using the Poissonian distribution to find the possible range of underlying average triggered earthquake rates corresponding to each integer number of triggered earthquakes observed for the different values of $T1$, we then obtain a full 98% confidence range of K from 0.0121 to 0.0279, where K is calculated for a mainshock magnitude average of M 5.4 (the average magnitude of our data set) and the production of $M \geq 4$ aftershocks per day.

Now, if we set $T1$ to 400 days, giving us the lowest background rate of 0.02 $M \geq 4$ earthquakes per day per mainshock, we have 11 mainshocks. This gives that from 0.5 to 1.0 days we expect a total background rate of $(0.02/2) \times 11 = 0.11$ background earthquakes, or an actual count of 0–1 earthquakes 98% of the time ($B1 = 0, B2 = 1$). This means that triggering will only be clear at 98% confidence if 11 mainshocks taken together can be expected to produce, 98% of the time, a total of at least 2 $M \geq 4$

aftershocks at 0.5–1 days and >72 km. Assuming the highest value of K (0.0279) we expect these mainshocks to produce 0.0015 $M \geq 4$ aftershocks/mainshocks over 0.5–1.0 days and ≥72 km, or a total of $(0.0015^{*}11) = 0.0165$ aftershocks, which translates to a single observed aftershock only ~1.6% of the time and 2 aftershocks only ~0.01% of the time. Thus statistically significant triggering at 0.5–1 days is unlikely to be observed, even if the triggering process is still occurring. We next try setting $T1 = 50$, increasing our data set to 67 mainshocks and the background rate to 0.035 $M \geq 4$ earthquakes/day/mainshock. In this case the expected number of background earthquakes over the observation period is 0–4, requiring a total of 5 triggered earthquakes for a clear triggering observation. Using the same value of K as before, we find that this larger set of mainshocks will only produce these ≥5 earthquakes to occur 0.1% of the time. In summary, triggering rates are expected to be so low in comparison to the background that it is no surprise that we do not observe significant triggering in our sample.

On the basis of the previous calculations, if we assume that triggering at >0.5 days and >72 km does in fact continue, although our data set does not allow us to prove it, then we can use the values of K calculated previously to find the probability that the 2005 Anza earthquake triggered the earthquake at Yucaipa 4.2 days later. Because our K value is referenced to M 5.4 mainshocks, we need to correct this to the M 5.2 magnitude of the Anza mainshock by multiplying by $10^{5.4-5.2} = 10^{-0.2}$ (Felzer *et al.*, 2004). We use the lowest value of K from the range given previously, because it is the closest to the value found for the majority of choices of $T1$. This gives us a triggering rate of 0.0045 $M \geq 4.0$ earthquakes per day at 4.2 days and >72 km. Substituting this into equation (3) and using the background seismicity rate for Anza given previously (e.g., for $T1 = 257$ days) gives a 14% ± 1% probability (98% confidence interval) that the Yucaipa earthquake was triggered by the Anza mainshock. Note that if the 2005 Anza and Yucaipa earthquakes had a smaller temporal separation, the probability of a triggering relationship would have been much higher. For a 1 hr separation, for example, the probability of triggering would have been about 89%, and for a 12 hr (half day) separation, the probability would have been about 36%.

Discussion

The size of an aftershock zone can appear misleadingly small if substantial effort is not taken to catalog small magnitude aftershocks using data recorded by robust seismic networks close to the source region. Our analysis of the 2005 M_w 5.2 Anza aftershock sequence illustrates how strongly our perception of the spatial extent of an aftershock sequences is shaped by monitoring. Traditionally, instrumentation and routine processing in southern California limit the detection of aftershocks to those larger than approximately M 2. For large mainshocks, even many M 2 aftershocks cannot be initially observed (Enescu *et al.*, 2007; Kilb *et al.*, 2007). If only the few $M \geq 2$ aftershocks of the 2001 and 2005 Anza mainshocks had been observed, these sequences would have appeared to cover a much smaller area than the area revealed when $M \geq 1.0$ or $M \geq 0.5$ aftershocks are included (Fig. 2). In fact, the clearly clustered area of $M \geq 2$ aftershocks are within the 1–2 mainshock fault length radii region previously assumed to be the limits of an aftershock zone. The dense instrumentation, careful processing, and low attenuation at Anza provide the unique opportunity to observe a much larger spatial extent of aftershocks (see Ⓔ the movies available in the electronic edition of *BSSA*). These observations clearly support the idea that the spatial footprint of aftershock zones can extend out to tens of kilometers, even after small or moderate mainshocks.

We emphasize that our results do not indicate that aftershocks routinely occur out to ten fault lengths whatever the magnitude of the mainshock, but rather that they can occur out to at least 50 km after moderate earthquakes. Felzer and Brodsky (2006) demonstrated that aftershock zone size does not scale with mainshock fault length, and they suggest that the perception that such scaling does exist is simply because larger mainshocks have more aftershocks and usually only the larger aftershocks (e.g., a small percentage of the total) can be identified. Felzer and Brodsky (2006) conclude that for mainshock magnitudes of at least M 2–6 aftershocks occur out to at least 50 km independent of the mainshock magnitude. The triggering of normal aftershocks out to large distances has also recently been found globally (Van der Elst and Brodsky, 2008).

Guided by observational limitations, aftershock zones containing normal aftershocks (presumably all triggered by the same physical mechanism) were previously expected to be limited in size because it was assumed that the aftershocks were triggered by static stress changes, which decay very quickly with distance. A number of recent articles, however, have found evidence that most early (and quite possibly later) aftershocks, at all distances, are likely triggered by the more slowly decaying dynamic stress changes (Kilb *et al.*, 2000; Parsons, 2002; Gomberg *et al.*, 2003; Prejean *et al.*, 2004; Felzer and Brodsky, 2006; Mallman and Zoback, 2007). One of the most convincing studies is the demonstration by Pollitz and Johnston (2006) that seismic events occurring near San Juan Bautista produced at least 10–20 times more aftershocks than nearby aseismic episodes with similar seismic moment release.

If most aftershocks are triggered by dynamic stress changes and if the triggering of some aftershocks at far distances is a standard occurrence, even for smaller mainshocks, then there could be a causal relationship when two earthquakes occur relatively close in time to each other, even if they are separated by a significant distance. In the case of the 2005 Anza–Yucaipa pair, we find a 14% ± 1% probability that Yucaipa was triggered by the Anza mainshock, which is not large, but is nonnegligible. Because of the rapid inverse power law decay of the aftershock rate, the probability of triggering would have increased substantially if the two earthquakes had been closer together in time (i.e., if the time

separation was 1 hr, the probability of a triggering relationship would have been about 89%).

Conclusions

Aftershocks of the 2005 M_w 5.2 Anza earthquake extended along ~50 km of the San Jacinto fault—a distance of over ten times the ~4.5 km fault lengths of the mainshock. This was viewed as unusual because it has been traditionally held that the normal aftershock zone extends only 1–2 fault lengths from the mainshock. Here, we demonstrate that the common perception of the aftershock zone size is highly colored by the sensitivity of the seismic network. At Anza, as a result of dense instrumentation and low attenuation, many aftershocks as small as M 0.5 and M 0.0 could be detected, and we have shown that this higher detection is sufficient to explain the extended appearance of the aftershock zone for the 2005 earthquake and also for an M_w 5.0 earthquake that occurred at Anza in 2001. Models of typical California aftershock sequences with aftershock detection as good as that at Anza appear similar to the Anza sequences, and the decay of aftershock density with distance from the mainshock fault planes at Anza is as rapid as for other mainshocks in California. These data support the hypothesis that aftershocks routinely occur over distances much greater than two mainshock fault lengths. The reason this extended aftershock zone is a relatively new idea is because it requires a sophisticated network and data cataloging team to capture and catalog the small earthquakes that make up most of the extended aftershock zones.

We also calculate the probability that the 2005 Anza M_w 5.2 mainshock triggered the 2005 Yucaipa M_w 4.9 earthquake, which occurred 4 days later at a distance of 72 km. Based on a 60 yr data catalog for the region, the long term probability of randomly having two magnitude ~4.9 earthquakes separated by 4 days or less is only ~3%. To estimate the probability that the Anza earthquake triggered the Yucaipa earthquake, we look at the triggering of $M \geq 4$ earthquakes at similar distances and times using 67 M 5–6 California earthquakes. We find triggering occurring (increase of observed seismicity over the background rate at $>98\%$ confidence) at distances ≥ 72 km out to times of 0.25–0.75 days after the mainshocks. At later times the triggering rate becomes too low to detect above the background rate with high confidence. If we assume that triggering is still occurring, and use Omori's law to extrapolate aftershock rates observed earlier than the 4.2 day separation between the Anza and Yucaipa events, we estimate a $14\% \pm 1\%$ probability that the Yucaipa event was triggered by the Anza mainshock.

Data and Resources

Earthquake catalog data were obtained from the Southern California Seismic Network (SCSN) and by personal communication with members from the ANZA seismic network team (http://eqinfo.ucsd.edu/deployments/anza/index.php, last accessed June 2007). Further information about the ANZA network operated by the Scripps Institution of Oceanography can be found at www.eqinfo.ucsd.edu. SCSN data were obtained from the Web page http://www.data.scec.org/catalog_search/date_mag_loc.php (last accessed June 2006). We also used $M \geq 4$ 1984–2006 catalog data from the Working Group on California Earthquake Probabilities catalog (Felzer and Cao, 2008).

Acknowledgments

We are grateful to two anonymous reviewers whose reviews were very helpful in making this article clearer and easier to read. Thanks also to *BSSA* associate editor L. Wolf. We also thank J. Hardebeck and S. Hough for U.S. Geological Survey (USGS) internal reviews and thorough and thoughtful comments, and A. and L. Felzer for editing and assistance. Funding for D. Kilb was provided by the Blasker-Rose-Miah Fund, which is part of the science and technology grants from the San Diego Foundation. We are grateful to those associated with the collection, analyses, and cataloging of the ANZA seismic network data and the Southern California Seismic Network data; without these data this work would not have been possible.

References

Abercrombie, R. E. (2000). Crustal attenuation and site effects at Parkfield, California, *J. Geophys. Res.* **105,** 6277–6286.

Agnew, D., and F. Wyatt (2005). Possible triggered aseismic slip on the San Jacinto fault, in *Southern California Earthquake Center Annual Meeting*, Palm Springs, California, September 2005.

Aki, K. (1965). Maximum likelihood estimate of b in the formula $\log n = a - bm$ and its confidence limits, *Bull. Earthq. Res. Inst., Tokyo Univ.* **43,** 237–239.

Bakun, W. H., and B. W. Joyner (1984). The M_L scale in southern California, *Bull. Seismol. Soc. Am.* **74,** 1827–1843.

Båth, M. (1965). Lateral inhomogeneities in the upper mantle, *Tectonophysics* **2,** 483–514.

Benioff, H. (1951). Earthquakes and rock creep: Part I: Creep characteristics of rocks and the origin of aftershocks, *Bull. Seismol. Soc. Am.* **41,** 31–62.

Berger, J., L. M. Baker, J. N. Brune, J. B. Fletcher, T. C. Hanks, and F. L. Vernon III (1984). The Anza array: A high dynamic range, broadband, digitally radiotelemetered seismic array, *Bull. Seismol. Soc. Am.* **74,** 1469–1481.

Brodsky, E. E., V. Karakostas, and H. Kanamori (2000). A new observation of dynamically triggered regional seismicity: Earthquakes in Greece following the August, 1999 Izmit, Turkey, earthquake, *Geophys. Res. Lett.* **27,** 2741–2744.

Das, S., and C. H. Scholz (1981). Off-fault aftershocks caused by shear stress increase?, *Bull. Seismol. Soc. Am.* **71,** 1669–1675.

Dieterich, J. A. (1994). Constitutive law for the rate of earthquake production and its application to earthquake clustering, *J. Geophys. Res.* **99,** 2601–2618.

Enescu, B., J. Mori, and M. Miyazawa (2007). Quantifying early aftershock activity of the 2004 mid-Niigata prefecture earthquake, *J. Geophys. Res.* **112,** doi 10.1029/2006JB004629.

Fay, N. P., and E. D. Humphreys (2005). Fault slip rates, effects of elastic heterogeneity on geodetic data, and the strength of the lower crust in the Salton Trough region, southern California, *J. Geophys. Res.* **110,** doi 10.1029/2004JB003548.

Felzer, K. R. (2006). Calculating the Gutenberg–Richter b value (Abstract S42C-08), *EOS Trans. AGU* **87,** no. 52 (Fall Meeting Suppl.), S42C-08.

Felzer, K. R. (2008). Calculating California seismicity rates, Appendix I, in *The Uniform California Earthquake Rupture*

Forecast (2) (UCERF 2), U.S. Geol. Surv. Open-File Rept. 2007-1437I, 42 pp.

Felzer, K. R., and E. E. Brodsky (2006). Decay of aftershock density with distance indicates triggering by dynamic stress, *Nature* **441,** 735–738.

Felzer, K. R., and T. Cao (2008). WGCEP historical California earthquake catalog, Appendix H, in *The Uniform California Earthquake Rupture Forecast (2) (UCERF 2), U.S. Geol. Surv. Open-File Rept. 2007-1437H*, 127 pp.

Felzer, K. R., R. E. Abercrombie, and G. Ekström (2003). Secondary aftershocks and their importance for aftershock prediction, *Bull. Seismol. Soc. Am.* **93,** 1433–1448.

Felzer, K. R., R. E. Abercrombie, and G. Ekström (2004). A common origin for aftershocks, foreshocks, and multiplets, *Bull. Seismol. Soc. Am.* **94,** 88–98.

Felzer, K. R., T. W. Becker, R. E. Abercrombie, G. Ekström, and J. R. Rice (2002). Triggering of the 1999 M_w 7.1 Hector Mine earthquake by aftershocks of the 1992 M_w 7.3 Landers earthquake, *J. Geophys. Res.* **107,** 2190, doi 10.1029/2001JB000911.

Glowacka, E., F. A. Neva, G. D. de Cossío, V. Wong, and F. Farfán (2002). Fault slip, seismicity, and deformation in Mexicali Valley, Baja California, Mexico, after the *m* 7.1 1999 Hector Mine earthquake, *Bull. Seismol. Soc. Am.* **92,** 1290–1299.

Gomberg, J. (2001). The failure of earthquake failure models, *J. Geophys. Res.* **106,** 16,253–16,263.

Gomberg, J., P. Bodin, and P. A. Reasenberg (2003). Observing earthquakes triggered in the near field by dynamic deformations, *Bull. Seismol. Soc. Am.* **93,** 118–138.

Gutenberg, B., and C. F. Richter (1944). Frequency of earthquakes in California, *Bull. Seismol. Soc. Am.* **4,** 185–188.

Hadley, D., and H. Kanamori (1979). Regional *S*-wave structure for southern California from the analysis of teleseismic Rayleigh waves, *Geophys. J. Int.* **58,** 655–666.

Helmstetter, A., and B. E. Shaw (2006). Relation between stress heterogeneity and aftershock rate in the rate and state model, *J. Geophys. Res.* **111,** doi 10.1029/2005JB0040077.

Helmstetter, A., and D. Sornette (2003). Båth's law derived from the Gutenberg–Richter law and from aftershock properties, *Geophys. Res. Lett.* **30,** 2069, doi 10.1029/2003GL018186.

Helmstetter, A., Y. Y. Kagan, and D. D. Jackson (2005). Importance of small earthquakes for stress transfers and earthquake triggering, *J. Geophys. Res.* **110,** B05S08, doi 10.1029/2004JB003286.

Helmstetter, A., Y. Y. Kagan, and D. D. Jackson (2006). Comparison of short-term and time-independent earthquake forecast models for southern California, *Bull. Seismol. Soc. Am.* **96,** 90–106.

Hill, D. P., P. A. Reasenberg, A. Michael, W. J. Arabaz, G. Beroza, D. Brumbaugh, J. N. Brune, R. Castro, S. Davis, D. dePolo, W. L. Ellsworth, J. Gomberg, S. Harmsen, L. House, S. M. Jackson, M. J. S. Johnston, L. Jones, R. Keller, S. Malone, L. Munguia, S. Nava, J. C. Pechmann, A. Sanford, R. W. Simpson, R. B. Smith, M. Stark, M. Stickney, A. Vidal, S. Walter, V. Wong, and J. Zollweg (1993). Seismicity remotely triggered by the magnitude 7.3 Landers, California, earthquake, *Science* **260,** 1617–1623.

Hill, D. P. (2008). Dynamic stresses, Coulomb failure, and remote triggering, *Bull. Seismol. Soc. Am.* **98,** 66–92.

Hough, S. E. (2005). Remotely triggered earthquakes following moderate mainshocks (or why California is not falling into the ocean), *Seism. Res. Lett.* **76,** 58–66.

Hough, S. E., and L. M. Jones (1997). Aftershocks: Are they earthquakes or afterthoughts?, *EOS Trans. AGU* **78,** 505–508.

Hough, S. E., J. G. Anderson, J. Brune, F. Vernon III, J. Berger, J. Fletcher, L. Haar, L. Hanks, and L. Baker (1988). Attenuation near Anza, California, *Bull. Seismol. Soc. Am.* **78,** 672–691.

Kilb, D., J. Gomberg, and P. Bodin (2000). Triggering of earthquake aftershocks by dynamic stress, *Nature* **408,** 570–574.

Kilb, D., V. G. Martynov, and F. L. Vernon (2007). Aftershock detection thresholds as a function of time: Results from the ANZA seismic network following the 31 October 2001 M_L 5.1 Anza, California, earthquake, *Bull. Seismol. Soc. Am.* **97,** no. 3, 780–792, doi 10.1785/0120060116.

King, N. E., and J. C. Savage (1983). Strain rate profile across the Elsinore, San Jacinto, and the San Andreas faults near Palm Springs, California, *Geophys. Res. Lett.* **10,** 55–57.

Main, I. (2006). A hand on the aftershock trigger, *Nature* **441,** 704–705.

Mallman, E. P., and M. D. Zoback (2007). Assessing elastic coulomb stress transfer models using seismicity rates in southern California and southwestern Japan, *J. Geophys. Res.* **112,** B03304, doi 10.1029/2005JB004076.

Nur, A., and J. R. Booker (1972). Aftershocks caused by pore fluid flow?, *Science* **175,** 885–887.

Ogata, Y. (1988). Statistical models for earthquake occurrence and residual analysis for point processes, *J. Am. Stat. Assoc.* **83,** 9–27.

Omori, F. (1894). On the aftershocks of earthquakes, *J. College Sci. Imp. Univ. Tokyo* **7,** 111–200.

Parsons, T. (2002). Global Omori law decay of triggered earthquakes: Large aftershocks outside the classical aftershock zone, *J. Geophys. Res.* **107,** 2199, doi 10.1029/2001JB000646.

Parsons, T. (2005). A hypothesis for delayed dynamic triggering, *Geophys. Res. Lett.* **32,** L04302, doi 10.1029/2004GL021811.

Pollitz, F. F., and M. J. S. Johnston (2006). Direct test of static stress versus dynamic stress triggering of aftershocks, *Geophys. Res. Lett.* **33,** L15318, doi 10.1029/2006GL026764.

Prejean, S. G., D. P. Hill, E. E. Brodsky, S. E. Hough, M. J. S. Johnston, S. D. Malone, D. H. Oppenheimer, A. M. Pitt, and K. B. Richards-Dinger (2004). Remotely triggered seismicity on the United States west coast following the M_w 7.9 Denali fault earthquake, *Bull. Seismol. Soc. Am.* **94,** S348–S359.

Reasenberg, P. A., and L. M. Jones (1989). Earthquake hazard after a mainshock in California, *Science* **243,** 1173–1176.

Richter, C. F. (1958). *Elementary Seismology*, W. F. Freeman, San Francisco.

Scholz, C. H. (1968). Mircrofractures, aftershocks, and seismicity, *Bull. Seismol. Soc. Am.* **58,** 1117–1130.

Schorlemmer, D., J. Woessner, and C. Bachmann (2006). Probabilistic estimates of monitoring completeness of seismic networks, *Seism. Res. Lett.* **77,** 233.

Silverman, B. W. (1986). *Density Estimation for Statistics and Data Analysis*, Chapman and Hall, New York.

Sornette, A., and D. Sornette (1999). Renormalization of earthquake aftershocks, *Geophys. Res. Lett.* **26,** 1981–1984.

Steacy, S., J. Gomberg, and M. Cocco (2005). Introduction to special section: Stress transfer, earthquake triggering, and time-dependent seismic hazard, *J. Geophys. Res.* **110,** B05S01.

Toda, S., R. S. Stein, P. A. Reasenberg, J. H. Dieterich, and A. Yoshida (1998). Stress transfer by the $M_w = 6.9$ Kobe, Japan earthquake: Effect on aftershocks and future earthquake probabilities, *J. Geophys. Res.* **103,** 24,543–24,565.

Utsu, T. (1961). A statistical study on the occurrence of aftershocks, *Geophys. Mag.* **30,** 521–605.

Van der Elst, N. J., and E. E. Brodsky (2008). Quantifying dynamic earthquake triggering in the near and far-field (Abstract S23C01), *EOS Trans. AGU*, **89,** no. 53 (Fall Meet. Suppl.), S23C01.

Vernon, F. L. (1989). Analysis of data recorded on the Anza seismic network, *Ph.D. Thesis*, Scripps Institution of Oceangraphy, University of California, San Diego.

Walker, K., D. Kilb, and G. Lin (2005). The 2001 and 2005 Anza earthquakes: Aftershock focal mechanisms, in *Southern California Earthquake Center Annual Meeting*, Palm Springs, California, September 2005.

Wells, D. L., and K. J. Coppersmith (1995). New empirical relationships among magnitude, rupture length, rupture width, rupture area, and surface displacement, *Bull. Seismol. Soc. Am.* **84,** 974–1002.

West, M., J. J. Sanchez, and S. R. McNutt (2005). Periodically triggered seismicity at Mount Wrangell, Alaska, after the Sumatra earthquake, *Science* **308,** 1144–1146.

Appendix

Solving for Southern California Direct Modified Omori Law Parameters

One of the important components of our ETAS simulations is the modified Omori law (Utsu, 1961), which gives the aftershock rate as a function of time. It has been shown that mainshock and aftershock magnitude may be incorporated into the equation and the law written as the aftershock rate, R, is given by

$$R = k10^{(M_{\text{main}}-M_{\text{aft}})}(t+c)^{-p}, \qquad \text{(A1)}$$

(Felzer *et al.*, 2002) where M_{main} is mainshock magnitude, M_{aft} is the magnitude of the smallest aftershock counted, and k, c, and p are constants. These constants are often used to describe the activity of the entire aftershock sequence—that is, the compilation of direct and secondary triggers. In ETAS modeling, however, the direct versions of these parameters must be used—that is, the parameters that describe the activity level, with time, of direct aftershock sequences only. The full aftershock sequences are then naturally formed as the direct aftershock sequence of each earthquake and the direct aftershock sequence of each of its aftershocks is simulated. Unfortunately, solving for the direct Omori law parameters is much more difficult than solving for parameters that describe full aftershock sequences.

To solve for the direct Omori law parameters for the ETAS simulation, we first need to make a distinction between the magnitudes M_{min} and M_{minS}. M_{min} is the true, but unknown, magnitude of the smallest earthquake in the system that produces aftershocks. M_{minS} is the smallest magnitude used to produce aftershocks in the ETAS simulation. A decrease in M_{minS} results in more accurate simulations, but the number of required calculations increases exponentially.

For our simulations, we use M_{minS} 0.5. The long term direct p value does not vary with M_{minS} (Sornette and Sornette, 1999), and so we use the value of 1.34, solved for by Felzer *et al.* (2003) for California. Because k and c, on the other hand, increase with M_{minS}, we start with $k = 0.0053$ and $c = 0.085$, which were solved for by Felzer *et al.* (2003) for M_{minS} 0, and then increase these parameters incrementally and independently (by steps of 0.0001 and 0.001, respectively) until the average number of aftershocks produced by 100 thirty-day ETAS simulations for an M 6.0 mainshock is the closest (linear difference) to $10^{M_{\text{main}}-1.2-M_{\text{minS}}}$ aftershocks, which is derived from Båth's Law (Richter, 1958; Båth, 1965; see, Felzer *et al.*, 2002; Helmstetter and Sornette, 2003).

We further adjust k and c, by the same increments as previously, to fit our observation that southern California $M \geq 5.5$ earthquakes (in our 1984–2006 database) have approximately 0.12 as many aftershocks from days 10 to 30 after the mainshock as from days 0 to 10. We also match the aftershock rates in the first 2 days, and the first 5 days, of the aftershock sequences of 62 M 4.7–5.7 southern California mainshocks occurring from 1984 to 2006. This mainshock magnitude range was chosen to span the magnitude of the 2005 M 5.2 Anza earthquake. The M 4.7–5.7 mainshocks chosen comprise all of the earthquakes in this magnitude range that occurred at least 1 yr after and/or four fault lengths away from any larger earthquakes, thus ensuring that their observed early aftershocks are primarily their own and not part of a larger aftershock sequence. We use aftershocks down to M 2 for the measurement; thus, most of the aftershocks measured are smaller than their mainshocks. We express the average aftershock rates, however, in terms of the predicted number of aftershocks, using the Gutenberg–Richter relationship, with magnitudes larger than or equal to their mainshock magnitude over a specified time period. This predicted rate is positive even if there were no observed aftershocks larger than the mainshock in individual sequences, and this convention allows the measured aftershock rate to be independent of mainshock and aftershock magnitude. We thus measure an average rate of 0.043 ± 0.036 aftershocks/mainshock over the first 2 days of the sequences, where error is given at the 98% confidence level solved from 500 bootstraps of the data, and a rate of 0.055 ± 0.03 aftershocks/mainshock over the first 5 days. In comparison, when we calculate ETAS simulations for the aftershock sequence of an M 5.2 mainshock with our final parameters for M_{minS} 0.5 (Table A1), we recover a 2 day aftershock rate of 0.0426 ± 0.0006 aftershocks/mainshock (1000 simulations run, 500 bootstraps used to obtain the 98% confidence error) and a 5 day total of 0.0532 ± 0.0008 aftershocks/mainshock. Thus, modeled and observed aftershock rates compare favorably.

Table A1

Direct Aftershock Parameters for Use in the ETAS Simulations

M_{minS}	k	p	c
0.5	0.0068	1.34	0.09

M_{minS} is the magnitude of the smallest earthquake used in the simulations. k, p, and c are modified Omori law parameters (equation 4).

U. S. Geological Survey
525 South Wilson
Pasadena, California 91106
(K.R.F.)

Institute of Geophysics and Planetary Physics
Scripps Institution of Oceanography
University of California, San Diego
La Jolla, California 92093-0225
(D.K.)

Manuscript received 15 September 2008